

High-precision In situ silicon isotopic analyses by MC-SIMS in olivine and low-Ca pyroxene

Johan Villeneuve^{1,*}, Marc Chaussidon², Yves Marrocchi¹, Zhengbin Deng², and E. Bruce Watson³

¹ Centre de Recherches Pétrographiques et Géochimiques, CNRS UMR 7358, Université de Lorraine, 15 rue Notre-Dame des Pauvres, Vandœuvre-lès-Nancy, 54501 France

² Institut de Physique du Globe de Paris, Université Sorbonne Paris Cité, CNRS UMR 7154, 1 rue Jussieu, Paris, 75238 Paris France

³ Department of Earth and Environmental Sciences, Rensselaer Polytechnic Institute, Troy, NY 12180 USA

*Corresponding author, johanv@crpg.cnrs-nancy.fr

Abstract

Rationale: High-precision determination of silicon isotopes can be achieved by *in situ* multi-collector secondary ion mass spectrometry. The analyses accuracy is however sensitive to ion yields and instrumental mass fractionations (IMFs) induced by the analytical procedure. These effects vary from an instrument to another, with the analytical settings, and with the composition and nature of the sample. Because ion yields and IMF effects are not predictable and rely on empirical calibrations, high-accuracy analyses require suitable sets of standards.

Methods: Here, we document calibrations of ion yields and matrix effects in a set of 23 olivine standards and 3 low-Ca pyroxene for silicon isotopic measurements in both polarities using Cameca IMS 1270 E7 and IMS 1280 HR2 ion probes set with the cesium or radiofrequency (RF) source.

Results: Silicon ion yields show (i) strong variations with the chemical composition, and (ii) an opposite behavior between the secondary positive and negative polarities. The magnitude of IMF along the fayalite-forsterite (olivine) series shows a complex behavior, increasing overall by $\approx 7\%$ (secondary positive) and $\approx 15\%$ (secondary negative) with increasing olivine Mg#. A drastic change in olivine IMF occurs at Mg# ≈ 70 in both polarities. The magnitude of IMF for low-Ca pyroxene from Mg# = 70-100 is almost constant in both polarities, i.e. $\approx 0.1\%$ in secondary positive and $\approx 0.15\%$ in secondary negative. Analytical uncertainties on individual analyses were $\pm 0.05\text{--}0.15\%$ (2 S.E.) with

both sources, and external errors for each standard material were $\approx \pm 0.05\text{--}0.5\%$ (2 S.E.) with the Cs source and $\approx \pm 0.03\text{--}0.15\%$ (2 S.E.) with the RF source.

Conclusions: The IMF effect of Si isotopes in silicates shows complex behaviors that vary with the chemistry and the settings of the instrument. We developed a suitable set of standards in order to perform high-accuracy *in situ* measurements of Si isotopes in olivine and low-Ca pyroxene characterized by varying chemical compositions by MC-SIMS.

Keywords: Secondary ion mass spectrometer, silicon isotopes, ion yield, matrix effects

Introduction

Natural stable isotopic variations result from various processes that affect geological materials during their formation. Because H, C, N, O, and S commonly show large isotopic fractionations, they have been widely used in Earth and planetary sciences during the last half-century. Owing to recent considerable improvements in analytical methods, high-precision isotopic measurements of a large number of typically less-fractionated elements (Mg, Si, Fe, Cr, Zn, *etc.*) are now possible, providing insights into various processes such as evaporation and condensation during planetary formation¹, igneous differentiation², or metal-silicate fractionation³. Among the instruments allowing *in situ* isotopic analyses, the latest generation of ion probes, allowing multi-collector secondary ion mass spectrometry (MC-SIMS), is the most versatile with unique advantages: (i) high spatial resolution (5–20 μm beam diameter and 1–2 μm depth); (ii) high sensitivity, allowing detection limits below the ppm level for most elements; (iii) high mass-resolution analysis, thus removing most isobaric interferences; and (iv) a good level of analytical precision, usually better than 1‰ at 2σ depending on the element analyzed^{4–7}. These advantages make ion probes powerful tools for studying isotopic fractionations in complex mineralogical assemblages and zoned minerals. Regardless of the technique used, high-precision *in situ* isotopic analyses have always been challenging and rely on the use of suitable reference materials. Ion probes measurements can be particularly sensitive to differences in ion yields between elements and to mass-dependent instrumental isotopic fractionation. This latter effect is usually referred to as instrumental mass fractionation (IMF) and corresponds to the difference between the natural isotopic composition of a sample and the value measured with the ion probe. Ion yield and IMF essentially depend on the physics of the mass spectrometer, the analytical settings, and the nature and composition of the sample, *i.e.* the so-called “matrix effects”⁷. Neither ion yields nor IMF effects are predictable by physical models; they thus require empirical calibrations based on appropriate mineral and glass standards^{8,9}.

Because the electronic and electrical and physical environment of an ion probe are, in theory, stable during an analytical session, IMF variations that limit the accuracy of *in situ* isotopic measurements are, for a given analytical setting, mainly due to matrix effects. IMF can be understood as an incomplete ionization and transmission of the isotopes of an element through the mass spectrometer; *i.e.* 100% ionization and transmission would eliminate IMF. Therefore, extraction and ionization yields of secondary atoms (or molecules) are sensitive to variations in the chemical composition and/or crystalline structure of samples^{8,10,11}. Indeed, the efficiency of breaking chemical bonds between atoms and the ionization of atoms in the plasma relies on the binding energies between atoms, *i.e.* chemical composition and structure, and the elemental concentrations in the plasma¹². Matrix effects are well known for ion probes, and previous studies have shown that IMF

variations can be estimated from empirical calibrations with various parameters describing changes in the chemical composition of the matrix. For instance, it has been shown that (i) IMF varies linearly with the mass-to-charge ratio of octahedral cations (e.g. Mn, Mg, Fe, Ti) as they impact the strength of the OH and OB bond^{13–15} for analyses of $^2\text{H}/^1\text{H}$ in micas and amphiboles and $^{11}\text{B}/^{10}\text{B}$ in tourmaline, (ii) IMF during $^{18}\text{O}/^{16}\text{O}$ analyses in silicates depends on the SiO_2 and FeO contents^{16–18}, (iii) IMF during $^{18}\text{O}/^{16}\text{O}$ analyses in carbonates depends on Fe, Mg, and Mn contents^{19,20}, and (iv) IMF during $^{30}\text{Si}/^{28}\text{Si}$ and $^{44}\text{Ca}/^{40}\text{Ca}$ analyses in $\text{CaO-MgO-Al}_2\text{O}_3\text{-SiO}_2$ (CMAS) glasses varies linearly with optical basicity²¹. Thus, for a given isotopic system, it is often possible to build an empirical calibration from measurements of a limited number of well-chosen standards, and interpolate IMF values for different (but related) compositions. This is particularly the case for minerals belonging to the same solid solution (e.g. olivine, garnet, and tourmaline) and glasses.

Silicon has three stable isotopes, ^{28}Si , ^{29}Si , and ^{30}Si , with mean abundances of 92.23, 4.67, and 3.10% respectively²². It is a major and ubiquitous element in the Solar System that mainly occurs in the tetravalent oxidation state to form silicate minerals or amorphous forms of silica in rocks. In low oxygen fugacity environments such as the solar nebula, it is believed to occur as divalent gaseous species SiO or SiS . Silicon also exists as Si^0 in metallic alloys in inclusions in meteorites and iron meteorites^{23–25} and presumably in the metallic cores of terrestrial planets. Silicon isotopic research has taken full advantage of the recent rise of new generation multi-collector inductively coupled plasma mass spectrometers as well as *in situ* analytical devices such as laser-coupled multi-collector inductively coupled plasma mass spectrometers and the latest generation multi-collector secondary ions mass spectrometers (referred hereafter as ion probes) such as the Caméca IMS 1270/1280 series. Ion probes are versatile mass spectrometers allowing *in situ* isotopic measurements of major and trace elements, isotopic mapping or depth isotopic profiles in solid material, through the use of a focalized and accelerated primary beam of O^- or Cs^+ ions with a spatial resolution from 50 nm to a few tenth of μm . These developments have allowed the use of Si isotopes to address various problems in Earth sciences such as the formation and metal-silicate differentiation of planetary bodies, magmatic differentiation during igneous processes, the biogeochemical cycle of silicon, and the weathering of the continental crust or past terrestrial environments³. The overall variability of Si isotopes in bulk terrestrial and extra-terrestrial samples does not generally exceed a few per mil, making reliable IMF corrections essential³. *In situ* Si isotopic measurements have been performed via SIMS for the past 30 years, first applied to presolar grains from primitive carbonaceous meteorites that yielded large mass-independent Si isotopic fractionations with $\delta^{30}\text{Si}$ variations of $\sim 2000\%$ ²⁶. These measurements were performed on first-generation ion probes, *i.e.* Caméca IMS 3f, that did not allow good analytical precision. With the development of large-radius ion probes, *i.e.*

Caméca IMS 1270 and 1280, that allow multi-collection capability, high mass resolution and high ion transmission, analytical uncertainties were significantly reduced and reproducibilities much better than 1‰ on $\delta^{30}\text{Si}$ values were obtained: *e.g.* $\sim \pm 0.7\text{‰}$ in silcretes²⁷, $\sim \pm 0.1\text{--}0.4\text{‰}$ in CMAS synthetic glasses^{21,28}, and $\sim \pm 0.3\text{‰}$ in quartz and precambrian cherts^{6,29–31}.

In the present study, we have characterized the ion yield and IMF variations for Si isotopes measured by SIMS in a set of 23 natural and synthetic olivine standards, 3 natural low-Ca pyroxene standards, and 2 quartz standards used as a reference. We show that ion yields and IMFs in olivine standards do not follow any simple trend and must be carefully characterized to avoid inappropriate sample corrections. In contrast, IMFs in low-Ca pyroxenes seem to evolve linearly with simple compositional parameters over restricted compositional ranges and thus are more predictable.

Nomenclature and analytical approach

Si isotopic compositions are reported using the classical delta notation as per mil (‰) variations of the $^{29}\text{Si}/^{28}\text{Si}$ or $^{30}\text{Si}/^{28}\text{Si}$ ratio in a sample normalized to that of the NBS28 (international quartz standard SRM 8546, provided by the National Institute of Standards and Technology):

$$\delta^{29,30}\text{Si} = \left[\frac{\left(\frac{^{29,30}\text{Si}}{^{28}\text{Si}} \right)_{\text{sample}}}{\left(\frac{^{29,30}\text{Si}}{^{28}\text{Si}} \right)_{\text{NBS28}}} - 1 \right]$$

The absolute Si isotopic composition of NBS28 used here is $^{29}\text{Si}/^{28}\text{Si} = 0.0508229$ and $^{30}\text{Si}/^{28}\text{Si} = 0.0335336$ ³². Because $^{29}\text{Si}/^{28}\text{Si}$ and $^{30}\text{Si}/^{28}\text{Si}$ ratios show similar behaviors in regard to IMF (except for the amplitude which is twice higher for $^{30}\text{Si}/^{28}\text{Si}$ ratios compared to $^{29}\text{Si}/^{28}\text{Si}$ ratios) only the $^{29}\text{Si}/^{28}\text{Si}$ ratio will be used herein. The IMF for $^{29}\text{Si}/^{28}\text{Si}$ is defined by:

$$a_{\text{instr}}^{29/28} = \frac{\left(\frac{^{29}\text{Si}}{^{28}\text{Si}} \right)_{\text{measured}}}{\left(\frac{^{29}\text{Si}}{^{28}\text{Si}} \right)_{\text{true}}},$$

and can be approximated to the first order by:

$$\delta^{29}\text{Si}_{\text{instr}} = \delta^{29}\text{Si}_{\text{measured}} - \delta^{29}\text{Si}_{\text{true}},$$

with

$$\delta^{29}\text{Si}_{\text{instr}} \approx \ln(\alpha_{\text{instr}}^{29/28}).$$

Our in-house quartz standards (NL615 and Sonar) were measured and used as an internal reference to allow comparison between analytical sessions and to follow the stability of the ion probes (Fig. 1), *i.e.* $\delta^{29}\text{Si}_{\text{norm}}$ values are normalized to NL615 or Sonar (Tables 2, 3; Fig. 3).

In the case of our study, the Si ion yield is expressed as the efficiency with which Si atoms from a given matrix are sputtered, ionized, and transmitted to the mass spectrometer:

$$^{28}\text{Si yield} = ^{28}\text{Si}^{+,-} / [\text{SiO}_2]$$

with $^{28}\text{Si}^{+,-}$ the count rate of ^{28}Si ions in positive or negative polarity depending on the primary ion source used and $[\text{SiO}_2]$ the SiO_2 content of the sample. The count rate of $^{28}\text{Si}^{+,-}$ was normalized to the primary beam intensity (expressed in nA) and thus is given in counts/s/nA.

We use the Mg number parameter to characterize ion yield and IMF variations, expressed as:

$$\text{Mg\#} = \frac{[\text{Mg}]}{[\text{Mg}] + [\text{Fe}]},$$

with $[\text{Mg}]$ and $[\text{Fe}]$ the Mg and Fe contents in atomic percent. Mg# describes olivine compositions along the solid solution from the magnesian (forsterite, Mg# = 100) to the ferroan endmember (fayalite, Mg# = 0) or low-Ca pyroxene compositions from enstatite (Mg# = 100) to ferrosilite (Mg# = 0).

We studied a set of 2 in-house quartz standard, 23 olivines (9 synthetic⁷ and 14 natural olivines³³) spanning nearly the entire Mg# range from fayalite to forsterite, including two slightly different San Carlos olivine grains, and 3 low-Ca pyroxenes with Mg# from 70 to 100. The 2 sets of natural and synthetic olivine have already been characterized and are used for Mg and Fe isotopes measurements^{7,33}. The chemical compositions of these samples have been precisely determined and are summarized in Table 1^{7,33}. The Si isotopic compositions of synthetic (determined from the started silica powder: Alfar Aesar amorphous silica powder, lot number D13Y012) and San Carlos olivines, quartz, and low-Ca pyroxenes are given in Table 1³⁴. The true Si isotopic compositions of the other olivines are not known, but since samples with chemical compositions close to San Carlos olivine or

the synthetic olivines, *i.e.* with similar matrix effects, show identical (within analytical errors) $\delta^{29}\text{Si}$ and $\delta^{30}\text{Si}$ values measured with the ion probe, we expect that they yield similar Si isotopic compositions (Table 1). This assumption is strengthened by the fact that the overall variation of $\delta^{30}\text{Si}$ values in terrestrial igneous, magmatic, and mantellic rocks does not exceed 0.4‰³ and is thus negligible relative to the overall IMF observed on the ion probe (~15‰, Table 2). Therefore, the Si isotope value for San Carlos olivine ($\delta^{30}\text{Si}_{\text{true}} = -0.3 \pm 0.04$ and $\delta^{29}\text{Si}_{\text{true}} = -0.16 \pm 0.02$)³⁴ is considered at first order the real value for all unknown olivine samples (Table 1).

Isotopic analyses were performed on the multi-collector Cameca IMS 1270E7 and 1280HR instruments at CRPG-CNRS (Nancy, France) during 4 different analytical sessions. We used primary Cs^+ and O^- beams to characterize the ion yields and IMFs of Si isotopes in positive and negative polarity.

Cs source settings

Samples were sputtered with a ~5 nA intensity and ~15-20 μm diameter primary Cs^+ beam set in Gaussian mode (the size of the primary beam is controlled by the primary column lenses and the primary intensity distribution is gaussian) and accelerated at 10 kV. Secondary negative $^{28,29,30}\text{Si}^-$ ions were accelerated at 10 kV and analyzed in multi-collection mode on three off-axis Faraday cups (L'2, C, and H1, respectively). Charge accumulations on the sample surface were neutralized by the use of an electron gun. The mass resolving power (MRP) was set at $M/\Delta M = 5000$ (slit 2 - 250 μm - on the multicollection) using the entrance opened at 120 μm ; at this MRP, interferences on different masses are completely resolved. The transfer magnification was set at 100 μm to insure an efficient transmission of secondary ions. The field aperture was set at 2000 μm and the energy slit was closed at 40 eV in order to remove most of lens aberrations and secondary ions with too high energy. The typical vacuum during analysis was 5×10^{-9} tor. Yields of the amplifier electronic cards of the Faradays cups were calibrated at the beginning of each analytical session. Automatic centering of the transfer deflectors and mass was implemented in the analysis routine. A $10 \times 10 \mu\text{m}$ raster was applied to the primary beam to ensure flat-bottomed pits. Measurements typically consisted of a 90-s pre-sputtering during which electric noise backgrounds of the Faraday cup are measured, automatic mass and beam centering, and 40 cycles of 4-s integrations separated by 1-s waiting times. Thus, each measurement took ~7 min. Under these conditions, the typical count rate for ^{28}Si , ^{29}Si and ^{30}Si in San Carlos olivine was $\sim 1.2 \times 10^8$, $\sim 6 \times 10^6$, $\sim 4 \times 10^6$ counts per second respectively, and the internal precision on $\delta^{29}\text{Si}$ value was ± 0.05 – 0.15 ‰ (2 σ standard error) depending on the sample. Repeated analyses of the NL615 quartz internal standard showed an external reproducibility of ± 0.2 ‰ (2 σ standard deviation, Fig. 1) and an external error of ± 0.04 ‰ (2 σ standard error on 25 data, Table 3).

Other samples were measured five to ten times and yielded external errors between ± 0.05 and $\pm 0.5\%$ (2σ standard error, Table 3).

Radiofrequency source settings

Samples were sputtered with a ~ 40 nA intensity and ~ 10 - 15 μm diameter primary O^- beam set in Gaussian mode and accelerated at 13 kV. As for the Cs settings, secondary positive $^{28,29,30}\text{Si}^+$ ions were accelerated at 10 kV and analyzed in multi-collection mode on the same 3 off-axis Faraday cups with MRP = 5000 (slit 2). Settings for the entrance and energy slits, as well as transfer magnification and field aperture were also the same. The typical vacuum during analysis was 5×10^{-9} tor. Relative yields of the amplifier electronic cards of the Faradays cups were calibrated at the beginning of each analytical session. The analytical routine was the same as that for Cs settings, except that the automatic control of the energy centering was added to the routine in order to compensate for slight electrical charges changes on the sample surface. A 5×5 μm raster was applied to the primary beam to ensure flat-bottomed pits. Measurements typically consisted of a 90-s pre-sputtering during which the electric noise background of the Faraday cup is measured, automatic mass and beam centering, and 40 cycles of 4-s integrations separated by 1-s waiting times. Thus, each measurement took ~ 7 min. Under these conditions, the typical count rate for ^{28}Si , ^{29}Si and ^{30}Si in San Carlos olivine was $\sim 1.5 \times 10^8$, $\sim 7.5 \times 10^6$, $\sim 5 \times 10^6$ counts per second respectively, and internal precision on $\delta^{29}\text{Si}$ value was ± 0.05 – 0.10% (2σ standard error) depending of the sample. Repeated analyses of the Sonar quartz internal standard showed an external reproducibility of $\pm 0.11\%$ (2σ standard deviation, Fig. 1) and an external error of $\pm 0.03\%$ (2σ standard error on 20 data, Table 2). Other samples were measured five times and yielded external errors between ± 0.03 and $\pm 0.15\%$ (2σ standard error, Table 2).

Results and discussion

Si ion yields in olivine and low-Ca pyroxene

As shown in Fig. 2 and Tables 2 and 3, Si ion yields were clearly different between the different matrices studied (olivine, low-Ca pyroxene, and quartz) and the two primary ion sources used (one session using the RF source and three using the Cs source, producing positive and negative secondary ions, respectively). Indeed, Si ion yields with the Cs source were ~ 1.5 times better than with the O source for quartz, ~ 2.5 – 4 times better for low-Ca pyroxene, and ~ 2 – 7 times better for olivine standards (Fig. 2, Tables 2, 3). The Si ion yield evolves differently depending on the primary ion source; the $^{28}\text{Si}^+$ yield is stable with Mg# whereas the $^{28}\text{Si}^-$ yield slightly decreases in low-Ca pyroxene (Fig. 2). Olivine positive and negative ion yields similarly show opposite behaviors (Fig. 2).

Clear differences in ion yields between different matrices have been previously observed^{8,35}. In olivine, the evolution of the Si ion yield with Mg# is not linear; $^{28}\text{Si}^-$ yields increase until Mg# \approx 70–75, then decrease, whereas $^{28}\text{Si}^+$ yields decrease until the same SiO_2 content and then increase (Fig. 2). The same systematic for $^{28}\text{Si}^+$ was previously observed by Steele *et al.*³⁵ who indicated a minimum near Mg# = 65 (they did not investigate $^{28}\text{Si}^-$). Chaussidon *et al.*⁷ showed a similar systematic for the Mg ion yield in olivine with a change in behavior also at Mg# = 75. These complex changes of Si (and Mg) ion yields that affect both polarities are puzzling, since olivine is a solid solution with nothing particular in its chemical and structural properties at Mg# \approx 70–75. Since olivines have relatively restricted Si atomic contents, these changes must be in some way related to changes in their Fe and Mg contents, and therefore related to the ionic bonding between Si and Mg/Fe in the olivine structure. A kind of ‘competition’ between elements for ionization, which would enhance or suppress the emissivity of a specific element depending on its atomic environment during sputtering, has been previously proposed to explain some complex ionization behaviors^{8,9}. Thus, Chaussidon *et al.*⁷ proposed an empirical model based on the difference in enthalpies of atomization between Fe and Mg (used as a proxy for bond strength difference between Fe and Mg) that successfully fit Mg ion yields and IMF in olivine standards and CMAS and basaltic glasses. They showed that Mg ion yields and IMFs can be modeled with a two-component ionization including (i) a simple ionization process correlated with the Mg content and (ii) an enhanced ionization process amplified by the presence of Fe. A similar approach might be possible for Si ion yields in olivine, but the problem is more complex since Si ionization relies on the variations and interactions of both Mg and Fe. Therefore, we did not find a satisfactory way to model the evolution of the Si ion yield in olivine.

In low-Ca pyroxene, variations of ion yields are limited for Mg# between 70 and 100 for both $^{28}\text{Si}^+$ and $^{28}\text{Si}^-$ (Fig. 2). Such behavior is consistent with Steele *et al.* study³⁵.

IMF of Si isotopes in olivine and low-Ca pyroxene

To our knowledge, no systematic study of Si isotopic analyses in olivine and low-Ca pyroxene by SIMS has been reported in the literature. IMF variations in olivine as a function of Mg# are shown in Fig. 3 (complete data are available in Tables 1–3). Obviously, IMF in olivine strongly relies on the abundances of FeO and MgO. In secondary positive polarity, $\delta^{29}\text{Si}_{\text{instr}}$ decreases non-linearly by $\sim 3\text{‰}$ over the range Mg# \approx 10–70, then increases linearly by $\sim 6\text{‰}$ up to Mg# = 95 (Fig. 3). In secondary negative polarity, $\delta^{29}\text{Si}_{\text{instr}}$ value increases nonlinearly by $\sim 15\text{‰}$ from Mg# \approx 0 until reaching a plateau at Mg# \approx 70 (Fig. 3). IMF with the RF source can be fitted with a polynomial regression over the range Mg# \approx 10–70 and then a linear regression yielding residual of 0.16‰, whereas IMF with the Cs source can be fitted with a polynomial function yielding a residual of 0.22‰ (and even better over Mg# =

70–95; Fig. 3, Table 4). IMF with the Cs source is very well constrained above Mg# = 45 and is thus useful for IMF corrections in high-MgO olivines. In contrast, it may be preferable to analyze high-FeO olivines with the RF source, although the Si ion yield is lower. In any case, as with Mg and O isotopic measurements in olivine^{7,17}, a comprehensive set of standards is needed to avoid artificial isotopic fractionations and to ensure high precision IMF corrections for Si isotopes.

IMF in low-Ca pyroxene shows very small and linear variations with Mg# from 70-100 (Fig. 3). In secondary positive polarity, $\delta^{29}\text{Si}_{\text{instr}}$ value decreases linearly by $\sim 0.1\text{‰}$ whereas it increases linearly by $\sim 0.15\text{‰}$ in secondary negative polarity (Fig. 2). Therefore, IMF can be fitted with linear regressions yielding a residual of 0.01 for both sources.

Conclusions

Ion yields and IMFs in olivine show complex behaviors that rely on variations in both MgO and FeO content (Fig. 2, 3). In secondary negative polarity, IMF is well constrained above Mg# = 45, and particularly in the range Mg# = 70–100 where $\delta^{29}\text{Si}_{\text{instr}}$ value does not vary. Therefore, these settings are appropriate for high-accuracy Si isotopic analyses of high-MgO olivines. In contrast, $\delta^{29}\text{Si}_{\text{instr}}$ value does not vary much over Mg# = 0–70 in positive polarity; such settings are thus appropriate for analyses of high-FeO olivine. Ion yields and IMFs in low-Ca pyroxene are more predictable as they show limited variations over Mg# = 70-100.

Acknowledgment: This work was supported by PNP-INSU (French national program of planetology) and ANR CASSYSS (ANR-18-CE31-0010-01, PI J.V.). This is CRPG publication #2705.

References

1. Moynier F, Vance D, Fujii T, Savage PS. The Isotope Geochemistry of Zinc and Copper. *Rev Mineral Geochemistry*. 2017;82(1):543-600. doi:10.2138/rmg.2017.82.13
2. Dauphas N, John SG, Rouxel OJ. Iron Isotope Systematics. *Rev Mineral Geochemistry*. 2017;82(1):415-510. doi:10.2138/rmg.2017.82.11
3. Poitrasson F. Silicon Isotope Geochemistry. *Rev Mineral Geochemistry*. 2017;82:289-344. doi:10.2138/rmg.2017.82.8
4. Villeneuve J, Chaussidon M, Libourel G. Homogeneous Distribution of ^{26}Al in the Solar System from the Mg Isotopic Composition of Chondrules. *Science (80-)*. 2009;325(5943):985-988. doi:10.1126/science.1173907
5. Kita NT, Huberty JM, Kozdon R, Beard BL, Valley JW. High-precision SIMS oxygen, sulfur and

296 iron stable isotope analyses of geological materials: Accuracy, surface topography and crystal
 297 orientation. *Surf Interface Anal.* 2011;43(1-2):427-431. doi:10.1002/sia.3424

298 6. Marin-Carbonne J, Chaussidon M, Boiron MC, Robert F. A combined in situ oxygen, silicon
 299 isotopic and fluid inclusion study of a chert sample from Onverwacht Group (3.35Ga, South
 300 Africa): New constraints on fluid circulation. *Chem Geol.* 2011;286(3-4):59-71.
 301 doi:10.1016/j.chemgeo.2011.02.025

302 7. Chaussidon M, Deng Z, Villeneuve J, et al. In Situ Analysis of Non-Traditional Isotopes by SIMS
 303 and LA–MC–ICP–MS: Key Aspects and the Example of Mg Isotopes in Olivines and Silicate
 304 Glasses. *Rev Mineral Geochemistry.* 2017;82(1):127-163. doi:10.2138/rmg.2017.82.5

305 8. Shimizu N, Hart S. R. Applications of the ion microprobe to geochemistry and
 306 cosmochemistry. *Annu Rev Earth Planet Sci.* 1982;10:483-526.

307 9. Benninghoven A, Rudenauer FG, Werner HW. *Secondary Ion Mass Spectrometry: Basic*
 308 *Concepts, Instrumental Aspects, Applications and Trends.* United States: John Wiley and
 309 Sons, New York, NY; 1987. <http://www.osti.gov/scitech/servlets/purl/6092161>.

310 10. Reed SJB. Ion microprobe analysis a review of geological applications. *Mineral Mag.*
 311 1989;53:3-24.

312 11. Hinton RW. Ion microprobe trace-element analysis of silicates: Measurement of multi-
 313 element glasses. *Chem Geol.* 1990;83(1-2):11-25. doi:10.1016/0009-2541(90)90136-U

314 12. Eiler JM, Graham C, Valley JW. SIMS analysis of oxygen isotopes : matrix effects in complex
 315 minerals and glasses. *Chem Geol.* 1997;138:221-244.

316 13. Deloule E, France-Lanord C, Albarede F. D/H analysis of minerals by ion probe. *Geochem Soc*
 317 *Spec Publ.* 1991;3:53-62.

318 14. Deloule E, Chaussidon M, Allé P. Instrumental limitations for isotope measurements with a
 319 Caméca® ims-3f ion microprobe: Example of H, B, S and Sr. *Chem Geol Isot Geosci Sect.*
 320 1992;101(1-2):187-192.

321 15. Chaussidon M, Albarède F. Secular boron isotope variations in the continental crust: an ion
 322 microprobe study. *Earth Planet Sci Lett.* 1992;108(4):229-241.

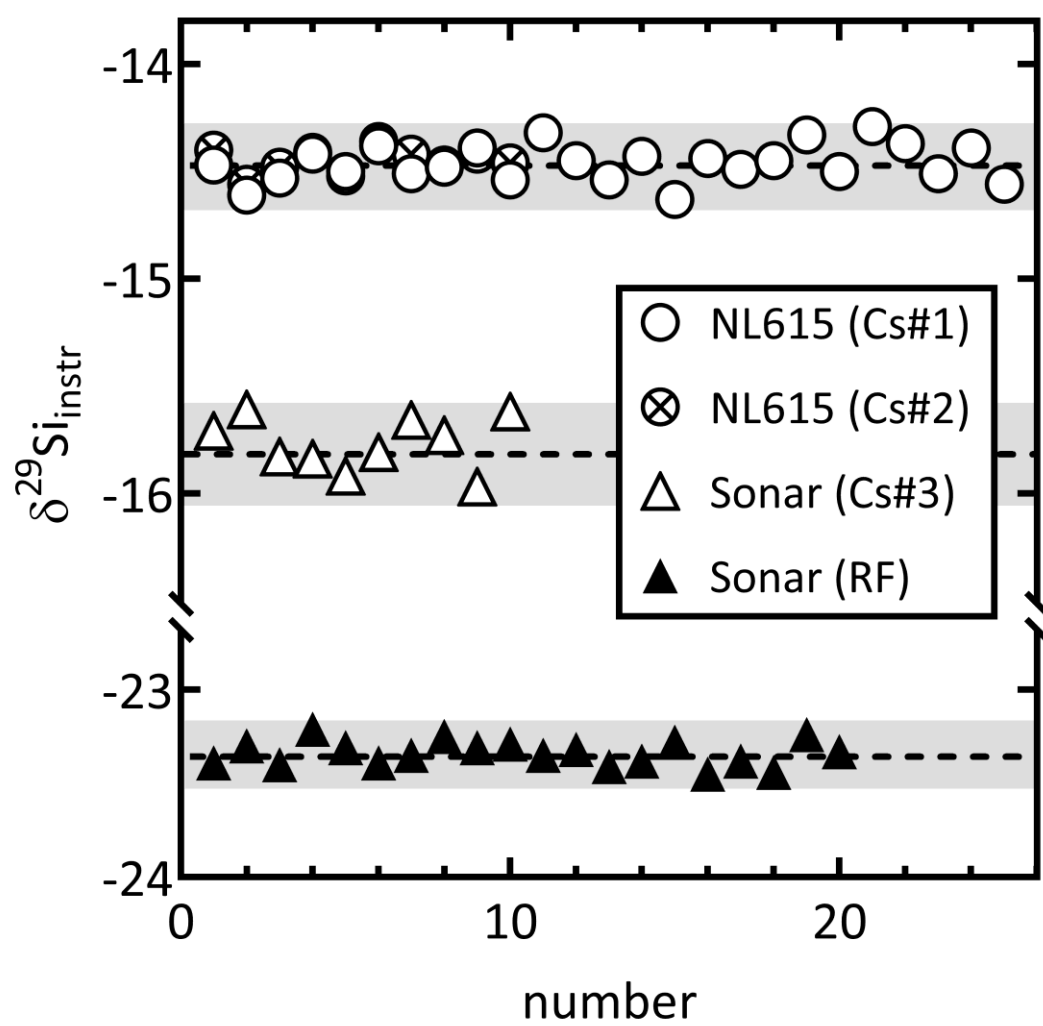
323 16. Chaussidon M, Libourel G, Krot AN. Oxygen isotopic constraints on the origin of magnesian
 324 chondrules and on the gaseous reservoirs in the early Solar System. *Geochim Cosmochim*

- 325 *Acta*. 2008;72(7):1924-1938. doi:10.1016/j.gca.2008.01.015
- 326 17. Isa J, Kohl IE, Liu MC, Wasson JT, Young ED, McKeegan KD. Quantification of oxygen isotope
327 SIMS matrix effects in olivine samples: Correlation with sputter rate. *Chem Geol*. 2017;458:14-
328 21. doi:10.1016/j.chemgeo.2017.03.020
- 329 18. Hartley ME, Thordarson T, Taylor C, Fitton JG, EIMF. Evaluation of the effects of composition
330 on instrumental mass fractionation during SIMS oxygen isotope analyses of glasses. *Chem*
331 *Geol*. 2012;334:312-323. doi:10.1016/J.CHEMGEO.2012.10.027
- 332 19. Rollion-Bard C, Marin-Carbonne J. Determination of SIMS matrix effects on oxygen isotopic
333 compositions in carbonates. *J Anal At Spectrom*. 2011;26(6):1285. doi:10.1039/c0ja00213e
- 334 20. Śliwiński MG, Kitajima K, Kozdon R, et al. Secondary Ion Mass Spectrometry Bias on Isotope
335 Ratios in Dolomite–Ankerite, Part I: $\delta^{18}\text{O}$ Matrix Effects. *Geostand Geoanalytical Res*.
336 2016;40(2):157-172. doi:10.1111/j.1751-908X.2015.00364.x
- 337 21. Tissandier L, Rollion-Bard C. Influence of glass composition on secondary ion mass
338 spectrometry instrumental mass fractionation for Si and Ca isotopic analyses. *Rapid Commun*
339 *Mass Spectrom*. 2017;31(4):351-361. doi:10.1002/rcm.7799
- 340 22. De Bievre P, Taylor PDP. Table of the isotopic compositions of the elements. *Int J Mass*
341 *Spectrom Ion Process*. 1993;123(2):149-166.
- 342 23. Ringwood AE. Silicon in the metal phase of enstatite chondrites and some geochemical
343 implications. *Geochim Cosmochim Acta*. 1961;25(1):1-13.
- 344 24. Keil K. Mineralogical and chemical relationships among enstatite chondrites. *J Geophys Res*.
345 1968;73(22):6945-6976.
- 346 25. Piani L, Marrocchi Y, Libourel G, Tissandier L. Magmatic sulfides in the porphyritic chondrules
347 of EH enstatite chondrites. *Geochim Cosmochim Acta*. 2016;195:84-99.
348 doi:10.1016/j.gca.2016.09.010
- 349 26. Zinner E, Ming T, Anders E. Large isotopic anomalies of Si, C, N and noble gases in interstellar
350 silicon carbide from the Murray meteorite. *Nature*. 1987;330:730-732.
- 351 27. Basile-Doelsch I, Meunier JD, Parron C. Another continental pool in the terrestrial silicon cycle.
352 *Nature*. 2005;433(7024):399-402. doi:10.1038/nature03217
- 353 28. Knight KB, Kita NT, Mendybaev RA, Richter FM, Davis AM, Valley JW. Silicon isotopic

- fractionation of CAI-like vacuum evaporation residues. *Geochim Cosmochim Acta*. 2009;73(20):6390-6401. doi:10.1016/j.gca.2009.07.008
29. Heck PR, Huberty JM, Kita NT, Ushikubo T, Kozdon R, Valley JW. SIMS analyses of silicon and oxygen isotope ratios for quartz from Archean and Paleoproterozoic banded iron formations. *Geochim Cosmochim Acta*. 2011;75(20):5879-5891.
30. Marin-Carbonne J, Chaussidon M, Robert F. Micrometer-scale chemical and isotopic criteria (O and Si) on the origin and history of Precambrian cherts: Implications for paleo-temperature reconstructions. *Geochim Cosmochim Acta*. 2012;92(March):129-147. doi:10.1016/j.gca.2012.05.040
31. Marin-Carbonne J, Robert F, Chaussidon M. The silicon and oxygen isotope compositions of Precambrian cherts: A record of oceanic paleo-temperatures? *Precambrian Res*. 2014;247:223-234. doi:10.1016/j.precamres.2014.03.016
32. Valkiers S, Ruße K, Taylor P, Ding T, Inkret M. Silicon isotope amount ratios and molar masses for two silicon isotope reference materials: IRMM-018a and NBS28. *Int J Mass Spectrom*. 2005;242(2-3):321-323. doi:10.1016/j.ijms.2004.11.027
33. Sio CKI, Dauphas N, Teng F-Z, Chaussidon M, Helz RT, Roskosz M. Discerning crystal growth from diffusion profiles in zoned olivine by in situ Mg-Fe isotopic analyses. *Geochim Cosmochim Acta*. 2013;123:302-321. doi:10.1016/j.gca.2013.06.008
34. Armytage RMG, Georg RB, Savage PS, Williams HM, Halliday AN. Silicon isotopes in meteorites and planetary core formation. *Geochim Cosmochim Acta*. 2011;75(13):3662-3676. doi:10.1016/j.gca.2011.03.044
35. Steele IM, Hervig RL, Hutcheon ID, Smith J V. Ion microprobe techniques and analyses of olivine and low-Ca pyroxene. *Am Mineral*. 1981;66(5-6):526-546.

Figures captions

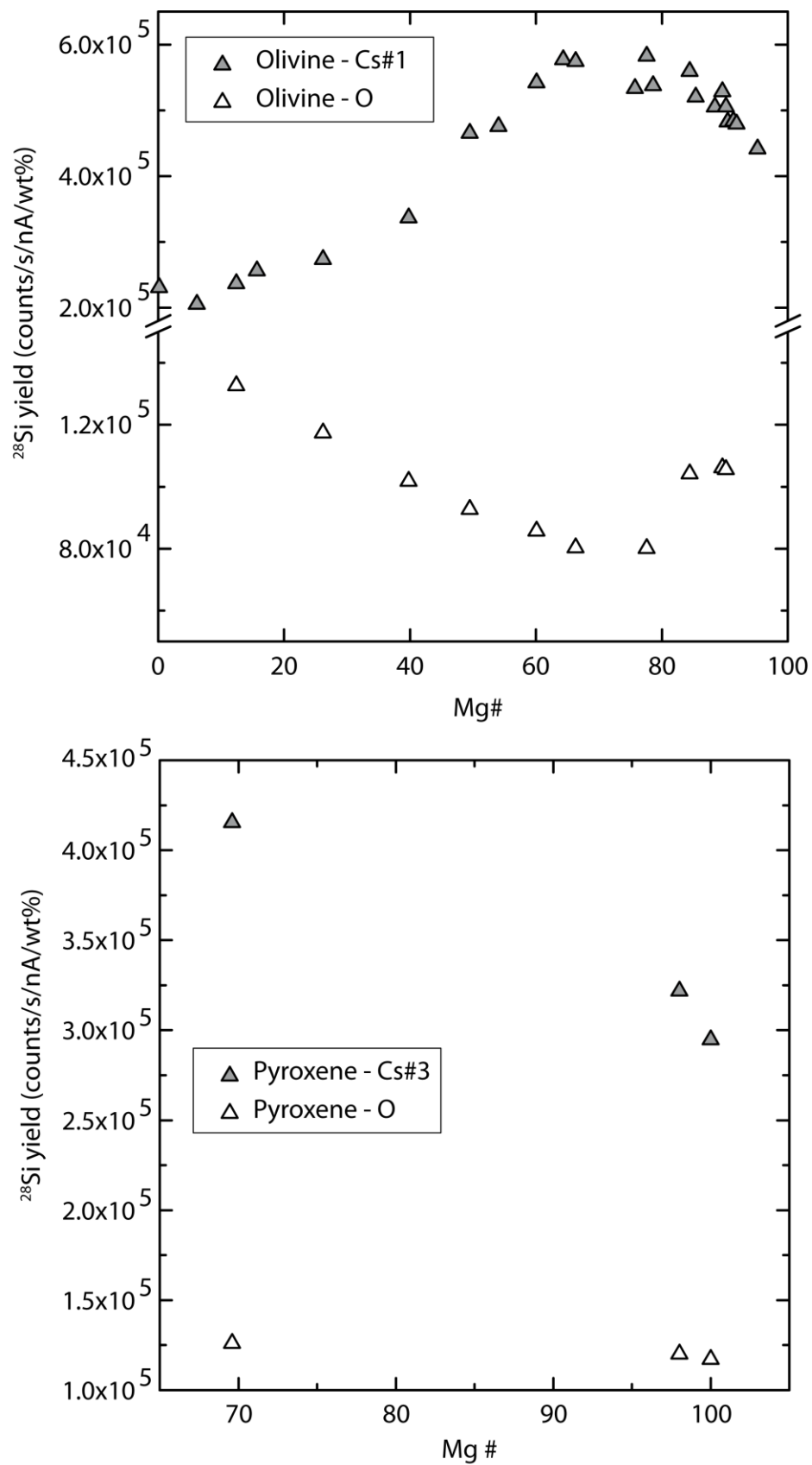
Fig. 1: Stability of NL615 and Sonar quartz standards over the different analytical sessions (see tables 2 and 3). Dashed lines and grey boxes correspond to average values and external reproducibilities (2σ standard deviation) respectively.



382

383

384 Fig. 2: ^{28}Si ion yields in both polarities as a function of Mg# in olivine (top) and in low-Ca pyroxene
 385 (bottom).



386

Fig. 3: $\delta^{29}\text{Si}_{\text{norm}}$ value as a function of Mg# in olivine (top) and in low-Ca pyroxene (bottom). The polynomial function regression is calculated from the olivine data of session #1 with the Cs source ($\delta^{29}\text{Si}_{\text{norm}} = -10.19 - 0.09 \times \text{Mg\#} + (1.38 \times 10^{-2}) \times \text{Mg\#}^2 - (1.79 \times 10^{-4}) \times \text{Mg\#}^3 + (6.57 \times 10^{-7}) \times \text{Mg\#}^4$). Data for olivine with the RF source are fitted with a polynomial function for $\text{Mg\#} < 65$ ($\delta^{29}\text{Si}_{\text{norm}} = -10.98 + 0.02 \times \text{Mg\#} - (8.69 \times 10^{-4}) \times \text{Mg\#}^2$) and a linear function for $\text{Mg\#} > 65$ ($\delta^{29}\text{Si}_{\text{norm}} = -30.60 + 0.25 \times \text{Mg\#}$). Data for low-Ca pyroxene are fitted with linear functions for both polarities, i.e. $\delta^{29}\text{Si}_{\text{norm}} = 5.95 + (4.90 \times 10^{-3}) \times \text{Mg\#}$ with the Cs source and $\delta^{29}\text{Si}_{\text{norm}} = -6.87 + (3.95 \times 10^{-3}) \times \text{Mg\#}$ with the RF source.

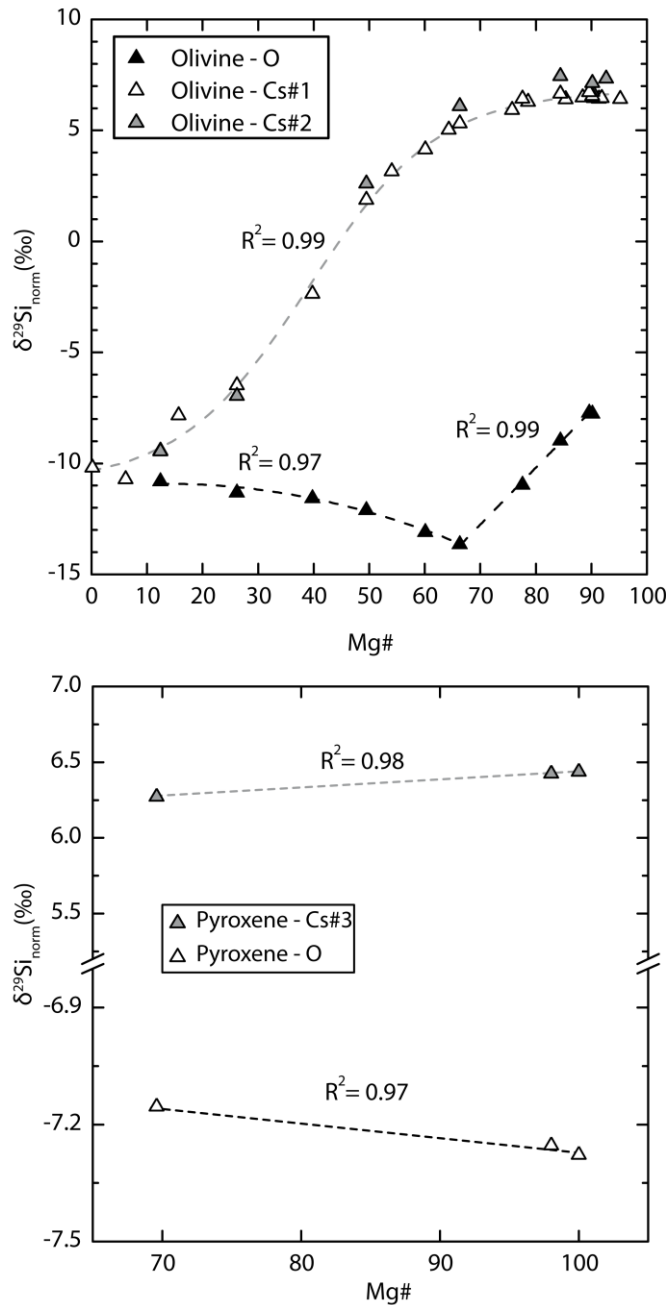


Table 1: Chemical compositions, bulk Si isotopic compositions normalized to NBS 28 (errors are 2 S.E., when available), Mg numbers of the studied standards. See text for details and parameter definitions. Isotopic compositions in *italic* are estimated (see text for details)

Standard	Al ₂ O ₃ [wt%]	MgO [wt%]	SiO ₂ [wt%]	CaO [wt%]	FeO _T [wt%]	Na ₂ O [wt%]	$\delta^{30}\text{Si}_{\text{true}}$ [‰]	$\delta^{29}\text{Si}_{\text{true}}$ [‰]	Mg#
Quartz									
NL 615	0.00	0.10	99.50	0.00	0.50	n.a.	-0.30 ± 0.03	-0.15 ± 0.03	n.a.
Sonar	0.00	0.00	100.00	0.00	0.00	n.a.	-0.38 ± 0.06	-0.21 ± 0.04	n.a.
Olivine (synthetic and natural) †									
Sio-Mg#0	n.a.	0.07	29.26	n.a.	67.21	n.a.	-0.30	-0.16	0.17
Sio-Mg#6	n.a.	2.46	29.99	n.a.	67.56	n.a.	-0.30	-0.16	6.14
Synth Watson #11	n.a.	5.06	30.60	n.a.	64.34	n.a.	-0.16 ± 0.07	-0.07 ± 0.01	12.40
Sio-Mg#16	n.a.	6.48	30.94	n.a.	62.58	n.a.	-0.30	-0.16	15.71
Synth Watson #10	n.a.	11.19	32.05	n.a.	56.76	n.a.	-0.16 ± 0.07	-0.07 ± 0.01	26.20
Synth Watson #9	n.a.	17.83	33.61	n.a.	48.56	n.a.	-0.16 ± 0.07	-0.07 ± 0.01	39.80
Synth Watson #8	n.a.	22.98	34.82	n.a.	42.20	n.a.	-0.16 ± 0.07	-0.07 ± 0.01	49.50
Sio-Mg#54	n.a.	25.55	35.42	n.a.	39.03	n.a.	-0.30	-0.16	54.09
Synth Watson #7	n.a.	29.05	36.25	n.a.	34.71	n.a.	-0.16 ± 0.07	-0.07 ± 0.01	60.10
SiO-Mg#64	n.a.	31.61	36.85	n.a.	31.54	n.a.	-0.30	-0.16	64.34
Synth Watson #6	n.a.	32.83	37.14	n.a.	30.04	n.a.	-0.16 ± 0.07	-0.07 ± 0.01	66.30
Sio-Mg#76	n.a.	38.97	38.58	n.a.	22.45	n.a.	-0.30	-0.16	75.75
Synth Watson #5	n.a.	40.22	38.88	n.a.	20.90	n.a.	-0.16 ± 0.07	-0.07 ± 0.01	77.60
Sio-Mg#79	n.a.	40.93	39.04	n.a.	20.03	n.a.	-0.30	-0.16	78.62
Synth Watson #4	n.a.	45.02	40.00	n.a.	14.98	n.a.	-0.16 ± 0.07	-0.07 ± 0.01	84.40
Sio-Mg#85	n.a.	45.74	40.17	n.a.	14.09	n.a.	-0.30	-0.16	85.39
Sio-Mg#88	n.a.	48.00	40.71	n.a.	11.29	n.a.	-0.30	-0.16	88.44
San Carlos Ol	n.a.	48.88	40.91	n.a.	10.21	n.a.	-0.3 ± 0.04 [‡]	-0.16 ± 0.02 [‡]	89.60
Synth Watson #1	n.a.	49.33	41.02	n.a.	9.65	n.a.	-0.16 ± 0.07	-0.07 ± 0.01	90.20
Sio-Mg#90	n.a.	49.55	41.07	n.a.	9.37	n.a.	-0.30	-0.16	90.49
Sio-Mg#91	n.a.	50.21	41.23	n.a.	8.57	n.a.	-0.30	-0.16	91.34
Sio-Mg#92	n.a.	50.63	41.33	n.a.	8.04	n.a.	-0.30	-0.16	91.89
CRPG SC Ol	0.03	50.94	41.32	0.07	7.21	0.01	-0.3 ± 0.04 [‡]	-0.16 ± 0.02 [‡]	92.68
Sio-Mg#95	n.a.	53.25	41.94	n.a.	4.81	n.a.	-0.30	-0.16	95.22
Pyroxene									
St Paul	1.39	24.18	52.30	1.58	19.01	0.06	-0.49 ± 0.05	-0.21 ± 0.04	69.60
Gold En	0.93	38.52	58.46	0.09	1.39	0.03	-0.07 ± 0.08	-0.06 ± 0.04	98.03
OEA En	0.04	39.88	60.62	0.00	0.00	0.04	-0.04 ± 0.04	-0.02 ± 0.04	100.00

†Chemical composition data from ^{7,33}. ‡Data from ³⁴

402 Table 2: Number of analyses (n), ^{28}Si yield, raw isotopic data, and IMFs normalized to NBS28 from
 403 MC-SIMS analyses with the RF source (positive secondary polarity)

Standard	n	^{28}Si yield [counts/s/nA/wt%]	$\delta^{30}\text{Si}_{\text{instr}}$ [‰]	2 S.E. [‰]	$\delta^{29}\text{Si}_{\text{instr}}$ [‰]	2 S.E. [‰]	$\delta^{29}\text{Si}_{\text{norm}}$ [‰]
RF source							
Quartz							
Sonar	20	1.90E+05	-41.88	0.05	-23.34	0.03	0.00
Olivine (synthetic and natural)							
Synth Watson #11	5	1.33E+05	-63.51	0.07	-34.14	0.06	-10.81
Synth Watson #10	5	1.17E+05	-64.31	0.29	-34.66	0.15	-11.32
Synth Watson #9	5	1.02E+05	-65.39	0.18	-34.90	0.10	-11.57
Synth Watson #8	5	9.27E+04	-66.31	0.09	-35.45	0.05	-12.11
Synth Watson #7	5	8.03E+04	-68.22	0.23	-36.43	0.10	-13.10
Synth Watson #6	5	1.04E+05	-69.07	0.21	-36.98	0.08	-13.64
Synth Watson #5	5	1.06E+05	-63.68	0.12	-34.31	0.09	-10.97
Synth Watson #4	5	1.06E+05	-59.92	0.14	-31.81	0.05	-8.47
San Carlos Ol.	5	1.33E+05	-57.05	0.05	-31.06	0.03	-7.72
Synth Watson #1	5	1.02E+05	-57.06	0.17	-31.10	0.14	-7.76
Pyroxene							
St Paul	5	1.26E+05	-55.73	0.17	-30.49	0.12	-7.15
Gold En	10	1.20E+05	-55.92	0.05	-30.59	0.05	-7.25
OEA En	5	1.17E+05	-55.99	0.09	-30.61	0.07	-7.28

404

405

406 Table 3: Number of analyses (n), ^{28}Si yield, raw isotopic data, and IMFs IMFs normalized to NBS28
 407 from MC-SIMS analyses with the Cs source (negative secondary polarity).

Standard	Session	n	^{28}Si yield [counts/s/nA/wt%]	$\delta^{29}\text{Si}_{\text{instr}}$ [‰]	2 S.E. [‰]	$\delta^{29}\text{Si}_{\text{instr}}$ [‰]	2 S.E. [‰]	$\delta^{29}\text{Si}_{\text{norm}}$ [‰]
Cs source								
Quartz								
NL615	#1	25	2.49E+05	-28.96	0.05	-14.45	0.04	0.00
NL615	#2	10	3.16E+05	-28.89	0.06	-14.45	0.03	0.00
Sonar	#3	10	2.18E+05	-29.68	0.11	-15.77	0.09	0.00
Olivine (synthetic and natural)								
Sio-Mg#0	#1	5	2.31E+05	-48.47	0.30	-24.63	0.33	-10.19
Sio-Mg#6	#1	5	2.05E+05	-49.54	0.43	-25.16	0.27	-10.71
Synth Watson #11	#1	5	2.37E+05	-47.32	0.50	-23.87	0.49	-9.42
Sio-Mg#16	#1	5	2.56E+05	-44.24	0.40	-22.32	0.22	-7.88
Synth Watson #10	#1	5	2.73E+05	-41.67	0.18	-20.93	0.11	-6.48
Synth Watson #9	#1	5	3.36E+05	-33.34	0.25	-16.80	0.15	-2.36
Synth Watson #8	#1	5	4.65E+05	-25.08	0.21	-12.57	0.12	1.88
Sio-Mg#54	#1	5	4.75E+05	-22.52	0.42	-11.29	0.26	3.16
Synth Watson #7	#1	5	5.42E+05	-20.59	0.18	-10.30	0.13	4.15
SiO-Mg#64	#1	5	5.77E+05	-18.97	0.20	-9.41	0.09	5.03
Synth Watson #6	#1	5	5.75E+05	-18.28	0.16	-9.14	0.10	5.31
Sio-Mg#76	#1	5	5.33E+05	-17.14	0.17	-8.52	0.10	5.93
Synth Watson #5	#1	5	5.83E+05	-16.31	0.17	-8.02	0.13	6.43
Sio-Mg#79	#1	5	5.37E+05	-16.54	0.14	-8.16	0.04	6.28
Synth Watson #4	#1	5	5.59E+05	-15.58	0.26	-7.79	0.17	6.66
Sio-Mg#85	#1	5	5.20E+05	-16.44	0.26	-8.05	0.10	6.40
Sio-Mg#88	#1	5	5.05E+05	-16.20	0.19	-7.96	0.06	6.49
San Carlos Ol	#1	5	5.29E+05	-15.67	0.17	-7.72	0.15	6.73
Synth Watson #1	#1	5	5.05E+05	-16.15	0.21	-7.96	0.12	6.49
Sio-Mg#90	#1	5	4.83E+05	-16.15	0.19	-7.98	0.16	6.46
Sio-Mg#91	#1	5	4.84E+05	-16.35	0.16	-8.01	0.07	6.44
Sio-Mg#92	#1	5	4.79E+05	-16.25	0.26	-7.98	0.16	6.46
Sio-Mg#95	#1	5	4.41E+05	-16.44	0.18	-8.03	0.17	6.42
Synth Watson #11	#2	5	2.84E+05	-47.06	0.22	-23.90	0.16	-9.46
Synth Watson #10	#2	5	3.19E+05	-42.41	0.55	-21.41	0.53	-6.96
Synth Watson #8	#2	5	5.35E+05	-23.70	0.24	-11.83	0.17	2.61
Synth Watson #6	#2	5	6.56E+05	-17.02	0.14	-8.35	0.13	6.10
Synth Watson #4	#2	5	6.49E+05	-14.36	0.12	-7.00	0.06	7.45
Synth Watson #1	#2	5	5.84E+05	-14.83	0.17	-7.31	0.10	7.14
CRPG SC Ol	#2	10	6.65E+05	-14.56	0.10	-7.12	0.03	7.33
pyroxene								
St Paul	#3	5	4.16E+05	-17.30	0.11	-9.48	0.08	6.29
Gold En	#3	5	3.22E+05	-17.01	0.16	-9.33	0.16	6.44
OEA En	#3	5	2.95E+05	-17.06	0.22	-9.32	0.08	6.43

408

409 Table 4: Coefficients of determination and average residuals of IMF ($\delta^{29}\text{Si}_{\text{norm}}$) as a function of Mg#
 410 for the different sessions and standard sets.

Data sets	No. of samples	$\delta^{29}\text{Si}_{\text{norm}}$ vs Mg#	
		R^2	Residuals*
Olivine - O	10	0.97-0.99	0.16
Olivine - Cs#1	23	0.99	0.22
Pyroxene - O	3	0.97	0.01
Pyroxene - Cs	3	0.98	0.01

411 * Residuals are expressed in ‰ and are calculated as: residual = $(\sum | \delta^{29}\text{Si}_{\text{norm}} - \delta^{29}\text{Si}_{\text{calc}} |) / (\text{no. analyses})$, with $\delta^{29}\text{Si}_{\text{norm}}$ the
 412 isotopic ratio measured for one sample and $\delta^{29}\text{Si}_{\text{calc}}$ the isotopic ratio of the same sample calculated from the regression
 413 curves.

414